

Studies on the energy and deep memory behaviour of a cache-oblivious, task-based hyperbolic PDE solver

Journal Title
XX(X):1–13
©The Author(s) 0000
Reprints and permission:
sagepub.co.uk/journalsPermissions.nav
DOI: 10.1177/ToBeAssigned
www.sagepub.com/

SAGE

Dominic E. Charrier¹, Benjamin Hazelwood¹, Ekaterina Tutlyaeva², Michael Bader³, Michael Dumbser⁴, Andrey Kudryavtsev⁵, Alexander Moskovsky², Tobias Weinzierl¹

Abstract

We study the performance behaviour of a seismic simulation using the ExaHyPE engine with a specific focus on memory characteristics and energy needs. ExaHyPE combines dynamically adaptive mesh refinement (AMR) with ADER-DG. It is parallelized using tasks, and it is cache efficient. AMR plus ADER-DG yields a task graph which is highly dynamic in nature and comprises both arithmetically expensive tasks and tasks which challenge the memory's latency. The expensive tasks and thus the whole code benefit from AVX vectorization, though we suffer from memory access bursts. A frequency reduction of the chip improves the code's energy-to-solution. Yet, it does not mitigate burst effects. The bursts' latency penalty becomes worse once we add Intel® Optane™ technology, increase the core count significantly, or make individual, computationally heavy tasks fall out of close caches. Thread overbooking to hide away these latency penalties becomes contra-productive with non-inclusive caches as it destroys the cache and vectorization character. In cases where memory-intense and computationally expensive tasks overlap, ExaHyPE's cache-oblivious implementation nevertheless can exploit deep, non-inclusive, heterogeneous memory effectively, as main memory misses arise infrequently and slow down only few cores. We thus propose that upcoming supercomputing simulation codes with dynamic, inhomogeneous task graphs are actively supported by thread runtimes in intermixing tasks of different compute character, and we propose that future hardware actively allows codes to downclock the cores running particular task types.

Introduction

The memory architectures in mainstream supercomputing (Intel-inspired architectures) become more and more inhomogeneous. We classify these trends into clocktick, vertical and horizontal inhomogeneity (Figure 1). Modern architectures can modify the chip frequencies of some components. Modern memory hierarchies are built in layers with the chip's registers on the top, persistent memory at the bottom, and caches in-between. This yields the vertical dimension. As access from the CPU registers to the main memory is very expensive, the caches hold data copies temporarily. Small intermediate memory layers can deliver data quick to the cores. Modern chips are predominantly multi-socket systems. This yields the horizontal dimension. Though the main memory and some intermediate memory layers are logically shared between all cores, the chip technically is split up into sets of cores with their own memories and memory controllers. Data access cost within one layer depends on whether data resides on the local

segment of memory or has to be fetched from memory technically associated to other sets of cores.

Neither vertical and horizontal nor frequency diversity are new. Their character however evolves and their impact on code performance increases. There are at least three recent hardware trends to consider: With an increase of core counts, non-uniform memory access (NUMA) effects gain importance. More cores and their caches have to

¹ Durham University, Department of Computer Science, Stockton Road, DH13LE Durham, Great Britain

² RSC Group, Kutuzovskiy av. 36, 121170 Moscow, Russia

³ Technische Universität München, Department of Informatics, Boltzmannstr. 3, 85748 Garching, Germany

⁴ University of Trento, Dipartimento di Ingegneria Civile Ambientale e Meccanica, Via Mesiano 77, 38123 Trento, Italy

⁵ Intel, 1900 Prairie City Rd, 95630 Folsom, United States

Corresponding author:

Tobias Weinzierl, Durham University, Department of Computer Science, Stockton Road, Durham, DH1 3LE, Great Britain

Email: tobias.weinzierl@durham.ac.uk

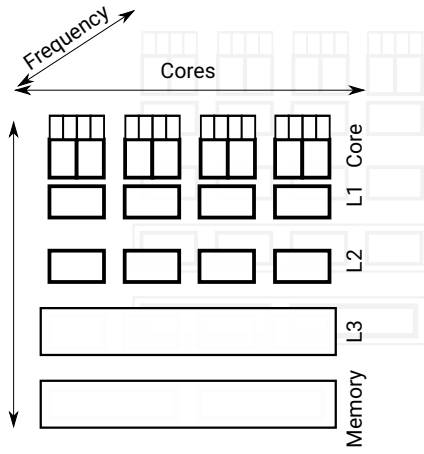


Figure 1. Vertical inhomogeneity of the data access cost, and thus speed, arises from multiple cache levels and different cache coherence strategies (inclusive vs. non-inclusive). With the Intel® Optane™ technology, main memory effectively becomes a fourth cache and an additional memory layer is added at the bottom. Horizontal inhomogeneity arises from the fact that memory is logically shared yet physically distributed. Further diversity stems from the fact that a core hosts multiple (hyper-)threads which in turn might accommodate multiple logical threads. A third diversity dimension is introduced by the opportunity to calibrate the cores' frequency.

be synchronised, while the pressure on the main memory increases. With the arrival of more inhomogeneous or new beyond-main memory storage technology (Intel® Optane™ technology or MCDRAM) which introduce new cache layers, as well as with the farewell of inclusive caching with the Intel® Xeon® Scalable processors (Skylake)—though likely to be compensated to some degree with the advent of mesh interconnects—we witness increased non-uniformity when it comes to memory accesses. With the opportunity to down- or upclock system components—either triggered by users or the energy controllers on board—we finally face further fluctuations in effective speed.

These hardware features are imposed on HPC simulations by the vendors. Despite co-design efforts, *algorithmic and hardware evolution seem to diverge for some of the most advanced simulation codes*. Code developer invest significant development time into the vectorization of their core compute kernels. Downclocking hits vectorization. Code developers invest significant time into a flexible task decomposition of their codes to uncover the maximum concurrency. Yet, modern numerics yield task graphs that have heterogeneous compute characteristics, non-predictable runtime cost and dependencies that change frequently. An example are predictor-corrector schemes with expensive predictors and cheap correctors, built on top of Newton- or Picard-iterations with dynamic termination criteria and dynamic adaptive mesh refinement (AMR). Horizontally diverse multicore systems challenge NUMA-aware scheduling. Finally, developers invest significant time

into cache blocking and compute routines of high arithmetic intensity which exploit all vector registers. New memory layers typically deliver improved bandwidth and storage size, but also increase latency. For embarrassingly parallel codes streaming data through the cores as we find them in machine learning, in-memory database systems (Boyandin et al. 2018) or dense matrix-matrix multiplications (Kudryavtsev 2018), latency poses a manageable challenge: threads accessing remote memory are postponed and switched with other threads. We “asynchronize” threads and memory accesses. Intel’s IMDT is explicitly built with this in mind (Figure 2). Indeed, moving data into the main memory upon request can even improve the performance, as moving the data into the “right” memory location eliminates NUMA penalties without complicated first-touch optimisations (Kudryavtsev 2018). Such a programming model, being similar to CUDA, is however problematic for codes which are tailored towards cache reuse, exploit all registers, and thus suffer from context switches.

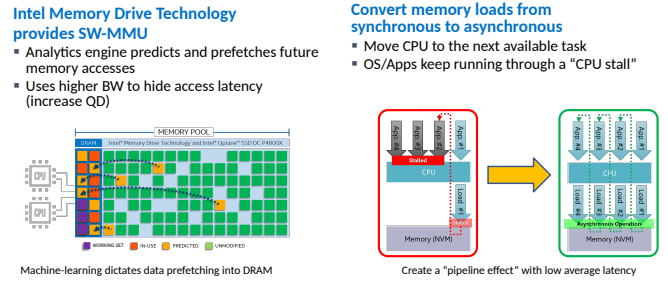


Figure 2. Intel® Optane™ SSD DC P4800X Series with Intel® Memory Drive Technology operation mode. It relies on software IP for memory management. Newer products such as Intel® Optane™ DC Persistent Memory are promised to integrate on DIMM form-factor and also to introduce a memory mode fully managed by the CPU without extra software; and hence smaller cost penalty.

Our case study on a complex AMR code with a non-homogeneous task pattern showcases flavours of this hardware-software divergence. It suggests that memory latency becomes a major showstopper. Unfortunately, (i) frequency modifications are ill-suited to tackle the latency problem—they help to improve the energy efficiency though—(ii) task/thread oversubscription is ill-suited to cure it either if data swapped out is not reliably backed up in the next-level cache, and (iii) additional memory layers amplify latency penalties. We however uncover that a heterogeneous task graph where tasks of different computational character are intermixed reduces the memory pressure and latency penalty. As a consequence, our code performs, from a memory point of view, better with dynamic AMR than with regular grids once the task character difference (compute- vs. memory-heavy) is reasonably high and dynamic AMR starts to mix those different tasks. This counter-intuitive

result is, to the best of our knowledge, novel, and our report also seems to be the first in a line that studies the impact of the Intel Optane technology on a non-trivial solver for partial differential equations (PDEs) from both a performance and an (memory) energy consumption view.

The case study is structured as follows: We give an overview over our benchmark code base ExaHyPE, before we phrase our research hypotheses. They circumscribe common expectations and will, in large parts, be falsified by our results. Our text next describes the two test machines. In the subsequent section, we benchmark the code's runtime characteristics, before we try to find evidence for our hypotheses. The findings are summarized in our conclusion and guide future work.

The ExaHyPE benchmark code

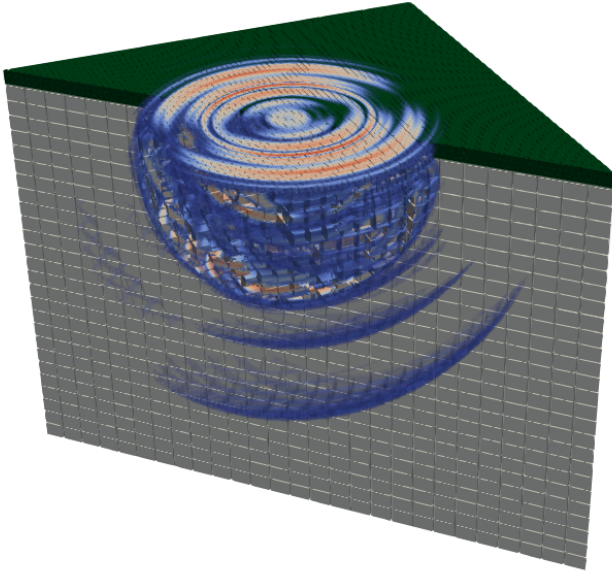


Figure 3. Cut through the solution of the LOH.1 below the surface. Waves propagate from this point but benchmark. A point source induces an “earthquake” just yield complicated patterns as the cubic domain contains two layers of different material (The SPICE Code Validation 2006). Regular grid visualization though the experiments run with both regular and dynamically adaptive meshes.

Our experiments study a strongly simplified and idealized earthquake scenario (Figure 3) realized through the ExaHyPE engine (Bader et al. 2014–2019). ExaHyPE solves hyperbolic differential equations in their first order formulation with ADER-DG. ADER-DG is a predictor-corrector scheme (Charrier and Weinzierl 2018; Dumbser and Käser 2006) which traverses a grid tessellating the computational domain and first computes per mesh cell a predicted solution evolution. This prediction is of the same order in time as the spatial order (typically $p \in \{3, 4, \dots, 9\}$)

and is determined implicitly. Solving such an implicit space-time problem is computationally possible as we neglect the solution in neighbouring cells. It is a cell-local prediction. The implicit solve of high order renders the predictor computationally intense. Riemann solves in a second step tackle the arising jumps in the predicted solutions along cell faces, before a corrector step sums up the result of the prediction and the Riemann solves. These two follow-up steps are arithmetically cheap.

ExaHyPE employs a dynamically adaptive Cartesian grid. It is constructed from a spacetree (Weinzierl and Mehl 2011; Weinzierl 2018). The term spacetree describes a generalization of the octree/quadtree concept. The meshing supports dynamically adaptive grids which may change in each and every time step. On purpose, we thus neglect multi-node runs. They inevitably yield load balancing challenges which hide the per-node memory effects studied here. The mesh topology determines which ADER-DG tasks can be run in parallel (Charrier et al. 2018): All Riemann solves for example are embarrassingly parallel but require input from their two neighbouring cells. Along adaptivity boundaries, more than two cells are involved. As the adaptivity changes, every time step induces a different multicore task pattern, i.e. the sequence and structure of parallel work items never is the same between any two time steps. We do not have a invariant task graph.

Combining a predictor-corrector scheme with task-based parallelism implies that (i) very compute-intensive steps take turns with tasks that are computationally cheap; (ii) the memory demands change as dynamic mesh refinement allocates additional blocks in the main memory while mesh coarsening releases memory segments; (iii) the concurrency profile of the code is time-dependent and changing such that dynamic tasking with task stealing is required. To cope with these characteristics, our code base is subject to three optimizations.

Homogenization of the task execution

In ADER-DG, all cell-based (correction and prediction) tasks are independent of each other cells. All Riemann tasks are independent of each other, too. Between those types, dependencies exist: A predictor requires the input from the correction which in turn requires the result of $2d$ Riemann solves. Each Riemann solve requires input from the two predictions of adjacent cells.

ExaHyPE offers two task processing modes. In its basic variant, it first issues one type of task, processes these tasks (which are all independent of each other), and then continues with the next type of tasks. Per time step, it first spawns

all predictor tasks, then all Riemann tasks, and finally all corrector tasks. Dynamic adaptivity introduces additional grid modification tasks. Each sweep is homogeneous w.r.t. its compute profile. The total time step however exhibits inhomogeneous character. This scheme is equivalent to a breadth-first traversal of the task graph.

An alternative variant is the fused mode (Charrier and Weinzierl 2018). It issues a task as soon as its input data are available. A Riemann solve starts as soon as the predictions of the two adjacent cells become available—it does not wait for all predictions to terminate—and a corrector task is issued immediately once all $2d$ Riemann solves on the cell’s adjacent faces are solved. We issue tasks as soon as possible. This induces some overhead to find out whether a task is already ready. Yet, the latter approach allows the task runtime to orchestrate tasks of different type to run concurrently. This homogenizes, i.e. averages the character of the tasks over a time step. Though we have no absolute control on the processing order of the tasks—this is up to the task runtime—we may assume that the task graph is processed close to a depth-first order (Reinders 2007).

Temporal and spatial blocking

ADER-DG’s predictor inherently realizes spatial and temporal blocking of data accesses (Kowarschik and Weiß 2003): The expensive implicit solves are not run on the whole mesh but on a per-cell basis. This means many floating point operations are executed over a relatively small set of data. On top of this, ExaHyPE’s grid traversal localizes all data accesses further. It traverses the grid along a space-filling curve whose Hölder continuity yields a spatial and temporal locality of data accesses (Weinzierl 2018). If the result of a Riemann solve feeds into once adjacent cell, the probability that the second adjacent cell is processed shortly after is high. Together with the optimization resulting from the homogenization, ExaHyPE realizes a cache-oblivious algorithm, which fuses correction and prediction. These cell operations are executed directly after another and merged into one task.

Optimization of task core routines

ExaHyPE customizes the engine: As soon as architecture, number of equation unknowns, PDE term types and polynomial orders are known—as they are for our LOH.1 setup—an ExaHyPE preprocessor (toolkit) can rewrite the most time-consuming code parts into manually vectorized, tailored code kernels. For these, it employs AVX instructions, appropriate alignment and padding, as well as aggressive

function inlining: the application-generic engine machinery is rewritten without virtual function calls.

Research hypotheses

We consider our ExaHyPE benchmark to be a prime candidate to study and assess new memory hierarchies, as the code exhibits multiple characteristic properties of modern simulation software: First, high-order, locally implicit approaches are one popular way forward to exploit vectorization. Second, we expect many future simulation codes to consist of different task types. Computationally demanding tasks—the workhorses—take turns with other, cheaper tasks which are however mandatory for advanced numerics. We focus on a predictor-corrector scheme here. Another popular example for such an algorithmic imprint are multigrid codes with expensive fine grid smoothers and cheap coarse equation systems. Third, we expect the majority of future codes to exploit some kind of dynamic adaptivity to invest compute power where it pays off most. As a result, task graphs, memory footprint and compute facility needs are never invariant or temporarily homogeneous. Notably, we assume that proper a priori prefetching becomes very difficult or even impossible for the runtimes. Forth, we assume that cache blocking—realised here implicitly through a computationally heavy predictor which acts on one cell of the mesh only—removal of virtual function calls, padding, manual vectorization and so forth are state-of-the-art for any compute kernel.

By means of our non-trivial benchmark setup, we follow up on the following hypotheses:

1. A frequency increase of the compute units helps to improve the time-of-solution, while a frequency reduction improves the energy-of-solution ratio. It also weakens the latency penalty.
2. Task oversubscription helps to hide latency effects. The popular (light) oversubscription pattern from CUDA enters mainstream processors.
3. The increased latency introduced by additional memory layers (fourth-level cache) harms notably those runs that exhibit a strongly inhomogeneous data access pattern (dynamic AMR). In-hardware prefetching breaks down.

Benchmark setup and system

Our benchmark is run on the following server configurations. The first one is an Intel Xeon E5-2650V4 (Broadwell) cluster in a two socket configuration with 24 cores. They run at 2.4 GHz. TurboBoost increases this to up to 2.8 GHz,

but a core executing AVX(2) instructions might fall back to a minimum of 1.8 GHz to stay within the TDP limits (Microway 2018). Each node has access to 64 GB of 2.4 MHz TruDDR4 memory.

The second configuration is a dual-socket Intel Xeon Scalable Gold 6150 with 18 physical cores per socket, clocked at 2.70 GHz, and equipped with 192 GB of 2.7 MHz DDR4 memory (12 ranks of 16 GB modules). The chip may reduce the base clock frequency to 2.3 GHz for AVX2 and to 1.9 GHz for AVX-512 (WikiChip 2018). The other way round, Thermal Velocity Boost permits individual cores to upclock to up to 3.7 GHz temporarily.

In our experiments, the latter system is expanded with $6\times$ Intel DC Optane SSD P4800X, i.e. 375 GB, non-volatile memory. The SSDs are connected via PCIe-switch IC to the CPU, while the Intel Memory Drive Technology implements software-defined memory (SDM) on-top of the Intel Optane technology SSDs (cmp. Fig. 2). This Intel Memory Drive Technology (IMDT) uses part of the overall memory capacity from the DRAM for caching, prefetching, and endurance protection, i.e. the drives become transparently available to the operating system as system memory. Though our memory totals to roughly 1.4 TB, we stick to the default IMDT settings recommended by Intel which limits the available memory to $8\times$ the main memory. Larger ratios than 1 : 8 would lead to performance drops according to the vendor.

All shared memory parallelization relies on Intel’s Threading Building Blocks (TBB) (Reinders 2007) while Intel’s 2018 C++ compiler translated all codes. We use Likwid (Treibig et al. 2010) to read out hardware and energy counters made available through RAPL. On the Purley platform chip, we use energy sensors that are directly attached to the board.

Our experiments study the LOH.1 benchmark (Day and Bradley 2001; The SPICE Code Validation 2006) realized through the ExaHyPE engine (Bader et al. 2014–2019). LOH.1’s artificial setup splits up a cubic domain into two horizontal layers of material. An earthquake then is induced as point source inside the cube. Sensors close to the domain surface track incoming waves. While LOH.1 is artificial, it exhibits real-world simulation characteristics with its material transition, a source term and non-trivial inference and reflection patterns. To obtain high quality results at reasonable cost, a feature-based refinement criterion follows the steepest solution gradients and shocks. The mesh spreads from the point source.

Benchmark code characteristics

Automatic frequency alterations

We kick off our experiments with studies on the Broadwell chip. For statements on the code’s scaling, it is important first to understand the frequency behaviour under load. On Broadwell, a single or dual core setup drives the chip at around 2.5 GHz (Figure 4). If we however use all 24 cores and run our optimised code variant using AVX, the node is downclocked to around 2.165 GHz on average. If we manually disable AVX, the downclocking is less severe (2.35 GHz on average). For all-core loads, overclocking is not used of the chip’s own accord. We observe one core—predominantly being busy with task production and scheduling—to perform at close-to-nominal speed. All others clock down. Scalability graphs have to take the amortized downclocking into account.

Scalability

To assess the impact of frequency, horizontal and vertical diversity, it would make limited sense to benchmark serial or non-scaling code. Before we study our code’s memory and energy characteristics, we thus validate that the code scales reasonably on Broadwell (Figure 5). Qualitatively similar results arise on the Intel Xeon Scalable chip. This holds despite the significantly changed memory architecture.

As the corrector step is merged into the predictor in the fused scheme, we benchmark the fused scheme against the nonfused implementation and decompose the latter’s behaviour into the scaling of the Riemann solve and the scaling of the cell-wise operator (Figure 5) top. While the predictor scales perfectly for both $p = 5$ and $p = 7$ once we accept that the cores clock down, the Riemann solvers scale hardly at all. They are heavy on data movements, move many small chunks of data, and suffer from the AMR administration overhead which we did not remove from any plot. Furthermore, we exploit the first-touch policy to ensure that data is allocated following their cell associativity: all cell data plus all faces of this cell are allocated en bloc by the allocating thread. The Riemann solves however bring together data from two cells and thus suffer from NUMA effects. In the end, the combination of the three task types ends up in-between these two extreme cases. Fusion is robustly faster than the nonfused scheme. The higher the order the more dominating the predictor steps. The arithmetic intensity of the Riemann solves in contrast is close to p -invariant. We thus obtain better scaling overall when we increase the order.

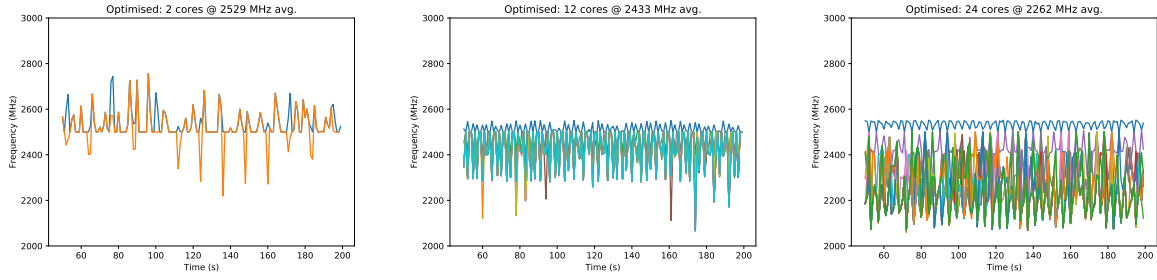


Figure 4. Broadwell's frequency choice per core for a dual core (left) a one-socket (middle) and a 24-core run (right). The caption gives the time-averaged frequency. All setups rely on code translated with AVX. Without the manual AVX optimisation, the average frequency is 2,616 GHz for two cores, drops to 2,454 GHz on a socket and finally to 2,409 GHz.

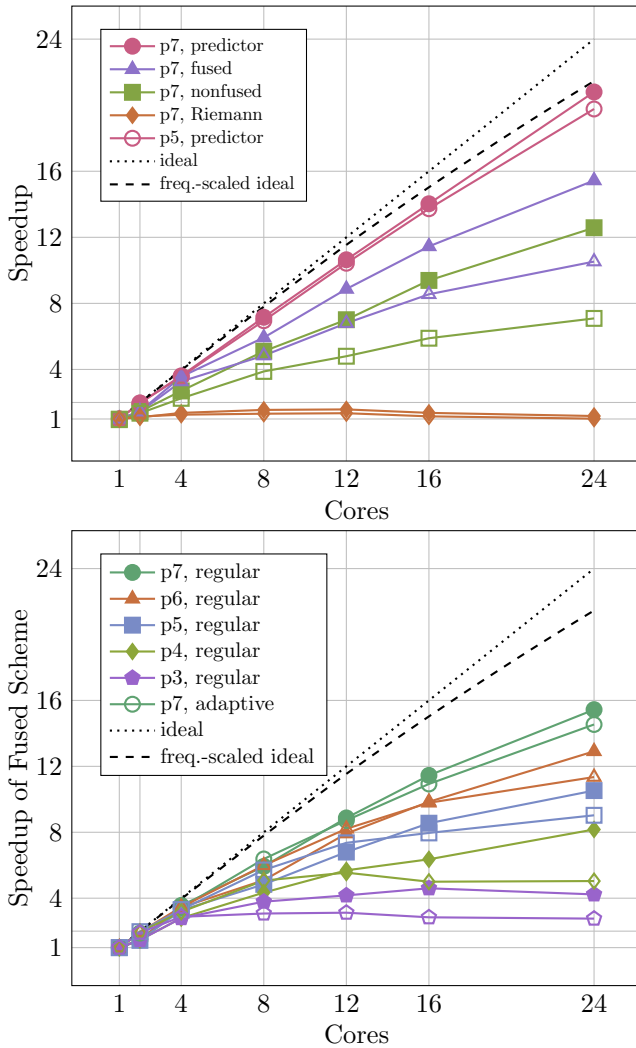


Figure 5. Code scalability on Broadwell for various orders and a $27 \times 27 \times 27$ grid. Top: Scalability of the isolated predictor and Riemann phase of the nonfused scheme plus overall scalability of the nonfused (straightforward) and the fused schemes for orders 5 and 7. Both an ideal linear speedup and a speedup calibrated with the observed frequency reduction are given. Bottom: Scalability of the fused scheme for orders 3—7. Regular grid runs are compared to a adaptive grids where a dynamic refinement criterion is allowed to add additional grid levels to the regular base grid.

Our experiments clarify that our code scales reasonably on one socket. The predictor “saves” the overall scalability. If we use the second half of cores too, the parallel efficiency deteriorates.

Observation 1. Strongly dynamic AMR codes with heterogeneous tasks suffer from multi-socket architectures. It might be reasonable to deploy one process/rank per socket, i.e. to give up on the idea of a larger shared memory system, to reduce NUMA effects.

Higher orders mitigate this effect, while dynamic adaptivity makes it slightly worse. Dynamic adaptivity is not for free. Further increases of the mesh resolution n (growing the mesh with $\mathcal{O}(n^d)$ for regular grids) or polynomial order (increase in $\mathcal{O}(n^p)$) are impossible due to memory limits on Broadwell. Our benchmark quickly is caught in a strong scaling regime. This observation is typical for many HPC codes working with dynamically adaptive meshes. They do not exhibit arbitrary concurrency.

Observation 2. To improve code scalability, increases of the polynomial order or mesh size are required. Such increases however are constrained by the memory available.

It does not come as a surprise that it is desirable to have more memory to be able to increase either the resolution, i.e. to shift the strong scaling regime, or p , i.e. to increase the arithmetic intensity (Hutchinson et al. 2016). While this favors the introduction of novel large-scale memory as provided through the Intel Optane technology, our observations suggest that any architectural extension that increases NUMA penalties affects the overall performance negatively.

Code characteristics and optimizations

If we rewrite our code into a fused variant where a task is immediately triggered once its input data become available, we obtain faster code. It robustly pays off to issue compute

tasks as soon as their input data is available and thus to overlap computationally demanding with memory-intense tasks. This observation is in line with implicit data access blocking as we find it in Intel’s TBB (Reinders 2007), where the task graph/tree is processed depth-first. We thus focus solely on the fused scheme from hereon.

Our benchmarking continues with performance counter measurements. Each test is done without any vectorization (disabled at compile time) and with full AVX2 vectorization. We observe a robust speed improvement through vectorization (Table 1). The reduction of the time-to-solution follows an increase of the Mflop rate. The positive vectorization impact is solely due to the high order prediction tasks which make up for the majority of the runtime. The higher the polynomial order, the higher the fraction of the runtime plus the higher the Gflop/s.

While the predictors are responsible for the Gflop/s, the solution update, which is fused with the predictor, delivers the memory throughput. It reaches around 25% of Stream TRIAD (McCalpin 1995) on Broadwell. Correcting the solution reduces the effective Mflop efficiency of this fused, cell-aligned task type. The vectorization success is diminished further by the fact that arithmetically intense tasks take turns with cheap Riemann solves. The runtime of the latter does not benefit from vectorization at all.

In none of our experiments, we have been able to observe any significant impact of the task character homogenization on the AVX downclocking. One might guess that intermixing computationally heavy with cheap tasks implies that not all cores run AVX at the same time, and the node thus does not throttle the speed as significantly. This however seems not to happen significantly. Figure 4 remains representative.

To characterize the cache usage, we measure per cache the request and the miss rate (Table 1). Request rate means number of requests divided by number of instructions. Miss rate means number of requests not served by a cache divided by number of instructions. From both rates, we can derive the miss ratio which is the ratio of cache accesses which have not been served by a particular cache.

The request rate of both L2 and L3 increases with increasing polynomial order. Furthermore, it is significantly higher for AVX-enabled code, while the request rate decreases rapidly over the cache levels. Our code’s aggressive cache blocking renders the dominating predictor cache-efficient. The predictor’s data does not fit into L1, but barely any misses hit through the last-level cache (LLC).

Our overall miss ratio however is high: Every time a piece of data is not found in the L2, the LLC cannot serve this request either with high probability. Though the

miss ratio decreases with increasing polynomial order, high ratios imply that we are neither bandwidth- nor compute-bound. This problematic behaviour stems from the Riemann solves. They pollute the caches through their low arithmetic intensity, small input data cardinality and NUMA effects and thus both are cache-inefficient themselves and pollute the following correctors. It is the re-filling of the caches with small chunks of data for the corrector/predictor steps which slows down the code. It is dominated by memory latency. The two steps themselves are memory-efficient.

The Intel Xeon Scalable chip amplifies all observed trends. The chip delivers higher performance—also due to the increased core count—and benefits from a decreased L2 miss ratio (Table 2), as the L2 cache per core is increased. However, changing from inclusive to non-inclusive caches and reducing the cache-per-core size makes the code yield an even higher L3 miss ratio. This results in a significantly increased memory bandwidth.

Observation 3. The code suffers from memory latency.

We obtain a reasonably high percentage of peak for a dynamically adaptive grid through the high order space-time predictor. The necessity to interwave it with cheap tasks however implies that we are overall neither compute- nor bandwidth-bound.

Frequency and energy analysis

AVX operations trade memory pressure for speed if data are accessed continuously, while they in turn induce a frequency reduction if the chip exceeds its energy/temperature thresholds (Figure 4). Our results (Table 3) validate that the reduction in time-to-solution compensates for problematic impact: With AVX, the executable delivers the results faster at lower energy footprint. This effect is the stronger the higher the polynomial order, i.e. the higher the arithmetic intensity of the heavy compute tasks.

We continue with experiments on our Xeon testbed and manually modify the frequency of the chip. Frequency alterations affect all standard components’ maximum speed, while intense AVX usage still might reduce the frequency. Our data tracks the time-to-solution and the energy consumption per simulation run (Figure 6).

Observation 4. Running a chip at maximum frequency is best in terms of time-to-solution. If energy per simulation however is the optimality condition, a significant reduction of the frequency is advantageous.

Our results are in line with reports on the best-case efficiency for Linpack if the total energy consumption has to be

Table 1. Hardware counters on Broadwell (24 cores) for a 27^3 grid. Scalar denotes no vectorization (`-no-vec -no-simd`) and no generation of vectorized inline assembler code. The top part presents the whole code characteristics if all three different task types are merged into each other. Below we split up the measurements into the phases prediction, Riemann solves and solution correction.

	Regular						Dyn. Adaptive					
	Scalar			AVX2			Scalar			AVX2		
	$p = 3$	$p = 5$	$p = 7$	$p = 3$	$p = 5$	$p = 7$	$p = 3$	$p = 5$	$p = 7$	$p = 3$	$p = 5$	$p = 7$
Avg. Time (s)	0.34	0.84	2.29	0.31	0.52	1.3	2.57	4.09	11.11	2.58	2.88	6.79
Gflop/s	12.3	32	41.7	12.8	47.9	74.3	3.7	18.4	37.1	5.7	23	58.1
L2 Request Rate (%)	6.55	9.27	8.80	8.52	16.34	19.78	5.09	7.56	7.99	6.79	14.93	18.16
L2 Miss Ratio (%)	13.76	14.43	18.95	10.37	15.28	19.96	17.12	16.91	18.26	11.92	13.63	17.59
L3 Request Rate (%)	0.09	0.04	0.04	0.11	0.20	0.28	0.05	0.05	0.04	0.09	0.17	0.28
L3 Miss Ratio (%)	29.38	7.43	8.85	60.69	20.91	13.40	28.23	14.15	9.86	44.55	24.26	11.57
Mem. Bandwidth (GB/s)	7.9	6.5	5.4	6.4	12	9.7	4.5	6.8	5.7	6.1	8.2	9.4
Avg. Time (s)	0.3	0.51	1.78	0.28	0.38	0.94	1.95	2.56	9.04	1.97	2.32	4.59
Gflop/s	11.8	42	54.3	11.8	26.9	93.1	5.5	22.3	51.8	4	24.5	66.1
L2 Request Rate (%)	6.49	8.69	8.92	9.21	17.17	18.17	5.08	8.43	8.63	7.14	14.24	18.32
L2 Miss Ratio (%)	9.58	16.07	18.79	8.26	15.56	22.49	13.37	15.35	15.77	8.90	17.68	20.48
L3 Request Rate (%)	0.02	0.04	0.04	0.05	0.19	0.28	0.03	0.04	0.03	0.06	0.16	0.25
L3 Miss Ratio (%)	25.48	4.64	6.84	41.80	2.99	3.96	27.42	11.22	10.98	29.54	8.06	5.54
Mem. Bandwidth (GB/s)	4.85	6.34	4.09	6.05	11.74	6.91	3.17	4.34	3.25	4.49	5.47	5.86
Avg. Time (s)	0.11	0.1	0.11	0.11	0.11	0.1	0.95	0.99	1.04	0.92	0.94	0.96
Gflop/s	0.6	3	9.4	0.6	3	8.6	0.5	3.8	15.6	0.2	1.1	2.8
L2 Request Rate (%)	9.62	9.91	8.32	8.32	14.37	18.76	3.61	3.03	6.45	3.37	5.32	8.07
L2 Miss Ratio (%)	17.18	16.42	17.15	16.65	16.07	19.71	20.43	20.08	5.29	23.54	20.26	21.85
L3 Request Rate (%)	0.10	0.05	0.05	0.17	0.30	0.28	0.08	0.05	0.02	0.09	0.10	0.16
L3 Miss Ratio (%)	30.97	21.59	12.72	33.23	18.92	9.96	24.76	23.86	19.27	28.34	26.17	14.61
Mem. Bandwidth (GB/s)	2	2.9	4.3	1.66	2.4	3.31	3.7	3.32	2.71	3.36	3.51	3.62
Avg. Time (s)	0.11	0.14	0.18	0.14	0.14	0.18	1.13	1.55	2.1	1.1	1.27	1.72
Gflop/s	2	6.6	12.5	1.8	6.4	13	1.2	5.3	15.6	0.6	2.1	5
L2 Request Rate (%)	5.61	6.51	8.10	16.06	19.20	25.79	3.69	3.53	7.22	5.59	9.01	13.64
L2 Miss Ratio (%)	22.32	19.64	14.67	26.43	20.56	17.73	25.49	21.58	7.54	26.93	23.27	21.36
L3 Request Rate (%)	0.10	0.05	0.05	0.32	0.34	0.42	0.08	0.08	0.04	0.13	0.24	0.26
L3 Miss Ratio (%)	39.82	34.55	33.17	61.23	46.50	41.84	35.39	38.22	32.61	37.58	43.81	39.93
Mem. Bandwidth (GB/s)	7.2	15.9	21.7	8.4	18	26.8	4.6	7.3	9.9	3.8	7.2	11.6

Table 2. Measurements from Table 1 for the Intel Xeon Scalable Gold running with all 36 cores. We show only data for the fused scheme without a breakdown into individual phases.

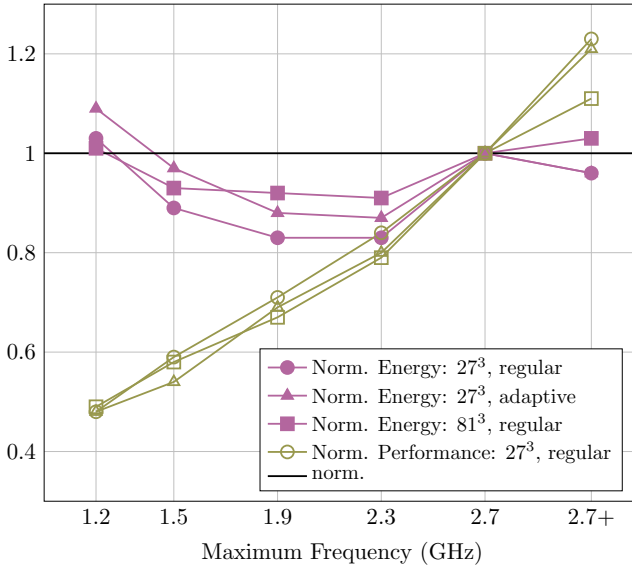
	Regular						Dyn. Adaptive					
	Scalar			AVX2			Scalar			AVX2		
	$p = 3$	$p = 5$	$p = 7$	$p = 3$	$p = 5$	$p = 7$	$p = 3$	$p = 5$	$p = 7$	$p = 3$	$p = 5$	$p = 7$
Avg. Time (s)	0.28	0.38	1.15	0.27	0.32	0.95	2.32	3.01	6.48	2.52	3.19	5.36
Gflop/s	14.6	62.5	86.7	22	100.9	156.4	7.3	32	74.6	8	32.8	95.3
L2 Request Rate (%)	4.82	5.55	7.64	9.31	15.64	21.68	5.81	5.66	8.76	11.06	18.78	22.00
L2 Miss Ratio (%)	8.25	4.10	11.46	9.25	7.35	12.27	12.86	4.31	9.27	11.41	3.70	12.44
L3 Request Rate (%)	0.03	0.02	0.03	0.11	0.06	0.16	0.06	0.01	0.03	0.15	0.08	0.17
L3 Miss Ratio (%)	55.04	60.71	14.22	85.55	75.49	59.23	37.52	45.68	11.69	56.32	63.04	47.92
Mem. Bandwidth (GB/s)	9.7	13.7	20.4	13.5	23.5	89.7	6.6	6.7	12.1	7.4	9.7	64.2

minimised (Glesser 2016). They also agree with ADER-DG experiments on tetrahedral meshes Breuer et al. (2015). More detailed studies however uncover three more insights: (i) A frequency alteration does not change the character of our latency challenge. We observe no flattening of the speed curve when we reduce the frequency. Notably, we have not been able to observe any statistically significant impact on the cache counters and thus latency effects when

we did alter the memory speed against the CPU (not shown). The memory’s auto mode choosing an appropriate memory speed is not outshadowed by any manual memory frequency tuning. (ii) For our heterogeneous task graphs, turbo boost techniques which allow cores to temporarily upclock yield significantly improved performance at a limited increase of energy hunger. (iii) With cache capacity moving closer to the chip, our cache-optimized algorithm also makes the chip

Table 3. Energy consumption per degree of freedom on Broadwell (24 cores) and Xeon Scalable (36 cores) for a typical run with a regular and a dynamic grid. The total energy plus the energy spent on the memory are given.

	Regular						Dyn. Adaptive					
	Scalar			AVX2			Scalar			AVX2		
	$p = 3$	$p = 5$	$p = 7$	$p = 3$	$p = 5$	$p = 7$	$p = 3$	$p = 5$	$p = 7$	$p = 3$	$p = 5$	$p = 7$
Total Energy (kJ)	1.46	5.24	15.54	1.29	3.02	9.01	27.57	41	96.84	22.24	28.42	53.7
Total Energy per DoF (mJ)	1.16	1.23	1.54	1.02	0.71	0.89	3.16	1.39	1.39	2.55	0.97	0.77
Energy DRAM (kJ)	0.49	1.25	3.06	0.43	0.78	1.79	6.96	9.03	19.12	5.42	6.62	10.64
Energy DRAM per DoF (mJ)	0.389	0.294	0.304	0.341	0.183	0.178	0.799	0.307	0.274	0.622	0.225	0.153
Total Energy (kJ)	3.24	6.41	17.77	2.85	4.63	13.32	36.46	46.68	123.74	51.75	46.49	91.48
Total Energy per DoF (mJ)	2.57	1.51	1.76	2.26	1.09	1.32	4.19	1.59	1.78	5.94	1.58	1.31
Energy DRAM (kJ)	0.17	0.25	0.69	0.17	0.25	0.87	1.83	2.04	4.95	2.72	2.42	4.9
Energy DRAM per DoF (mJ)	0.135	0.059	0.068	0.135	0.059	0.086	0.210	0.069	0.071	0.312	0.082	0.070

**Figure 6.** Energy and time-to-solution results for various CPU frequencies on the Intel Xeon Scalable machine for $p = 6$. We normalize the results against the default frequency of 2.7 GHz. 2.7+ GHz denotes a base clock of 2.7 GHz with 3.7 GHz TurboBoost enabled. The memory frequency is determined by the chip (auto modus).

spend more energy on the cores rather than the memory (Table 3).

Observation 5. Core frequency reductions—whether manually imposed or triggered through AVX—are *not* sufficient to mitigate latency effects.

Pinning, hyperthreading and latency hiding

Many HPC codes report pinning to be essential to achieve reasonable performance and to avoid NUMA pollution. We have not been able to confirm that pinning pays off for our code. No data are presented here, as no statistically pinning impact could be observed:

Observation 6. Runtimes with and without pinning can hardly be distinguished.

As our code is extremely cache efficient, data resides in the cache close to the core. If the system should decide to migrate a running task, the cache content has to be moved, too. However, a code with such extremely localized data access usually does not run into traditional cache conflicts and false sharing.

Hyperthreading and oversubscription are a popular technique for deep memory hierarchies (Figure 2) or systems where floating point units are shared between physical threads: Data requests by a thread which cannot served by a near cache trigger cache transfers. Meanwhile, the system swaps this thread with another compute thread until the data eventually has arrived. The compute facilities thus do not idle. This is similar to the streaming/high throughput compute paradigm in CUDA. While one thread uses the floating point capabilities, other threads can fetch/prepare all data for the subsequent AVX usage and queue to continue once the first thread “releases” the vector units.

On Broadwell, the techniques do yield performance improvements in our case (Figure 7). Starting from the Intel Xeon Scalable (Skylake) hardware generation however, they are counterproductive. They decrease the performance. This holds for all problem sizes.

Observation 7. Our code’s performance suffers from hyperthreading and thread oversubscription on systems with non-inclusive caches. Oversubscription is *not* a way forward to mitigate latency effects here.

The result is not a surprise once we take into account that the code relies heavily on data access localization and that individual tasks with their high arithmetic intensity already fill the close caches. Within one task, the code streams data through the AVX components. Switching tasks is expensive: It interrupts the AVX usage pattern of the current thread and induces further capacity misses on the close-by caches. If the data then still resides in a next-level cache, these runtime penalties are eventually compensated by the gain in

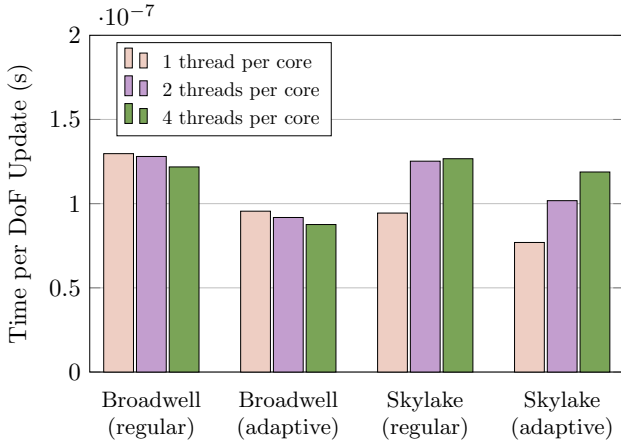


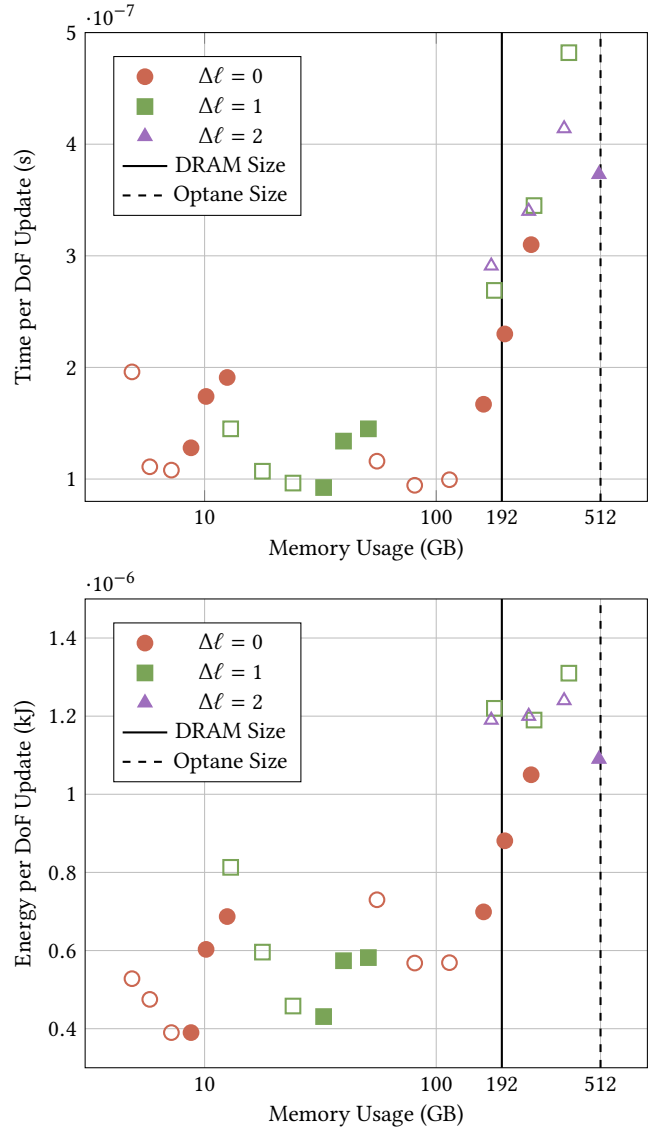
Figure 7. Characteristic $p = 7$ runs for both regular and adaptive meshes on the 36 cores of the Intel Xeon Scalable. We benchmark a one thread per core setup to oversubscribing with 2 (hyperthreading) or even 4 threads. The latter overbooks each hyperthread with two logical threads. The label Skylake identifies the Intel Xeon Scalable processor.

vector facility utilization. If swapped-out data however is not contained in a close-by cache—a situation likely with non-inclusive caching—swapping out logical threads becomes too expensive to be compensated. The effect is amplified by overhead necessary to administer the task queues and sequentialization and synchronization effects stemming from work stealing, e.g.

Additional deep memory (Intel Optane technology)

Finally, we scale up our problem size such that it does not fit into our conventional memory anymore. We use Intel Optane technology to accommodate this larger memory footprint. Hence, the conventional memory becomes a fully associative L4 cache. It is Intel’s hardware that is responsible for bringing data into and out of the cache. Agnostic of the particular data movement strategy, we may assume that high temporal and spatial locality (Kowarschik and Weiß 2003) in the memory accesses continues to be advantageous. Agnostic of the specific hardware properties, we may assume that “main memory cache misses” suffer from higher latency.

For the benchmarking, we start from two regular grids: 27^3 and 81^3 . These regular grids are denoted by $\Delta\ell = 0$, as we add 0 levels of dynamic adaptivity. Different to previous setups where, for reasonably large setups, memory constrains the dynamic adaptivity criterion and allows it to add at most one level of grid refinement, we now also conduct experiments with up to two additional resolution levels of dynamical adaptive meshes ($\Delta\ell \in \{1, 2\}$). All data is normalized against the real degrees of freedom and the



has to be done for all experiments here to obtain consistent data. Future versions of TBB will fix this stack size problem.

We spot a v-shaped cost profile for the setups fitting completely into memory (Figure 8). The cost per DoF update increases with p , an effect in practice more than compensated through the higher order of the approximation. Further to that, we see that this increase is more than made up as long as $p \leq 6$. Vector units are used more efficiently (cf. Tables 1 and 2). Once $p \geq 7$, the increase in cost also materialises in increased runtimes. The memory of the individual compute steps exceeds close caches (cf. L2 Request Rate in 2). We start to suffer from L2 or L3 cache misses. The v-pattern translates into energy per DoF update, too.

Once our regular grid setup exceeds main memory, we experience a runtime penalty. For the low order experiments, this penalty is significantly below a factor of three which would mirror the fact that the hardware has higher latency, too. With increasing orders, the penalty increases.

Observation 8. Trading bandwidth for latency does *not* work for our code. We suffer directly from increased latency.

With the Intel Optane technology, the v-pattern is distorted. The higher our bandwidth demands, the higher also the LLC misses and the higher the runtime penalty of the Intel Optane technology. We observe that the most aggressive adaptivity pattern $\Delta\ell = 2$ now yields a better cost per DoF update ratio than the more regular discretizations. The higher the polynomial order the more significant this effect. As the dynamically adaptive mesh intermixes memory-intense and arithmetically demanding tasks stronger, the runtime penalty induced by the Intel Optane technology is more significant for the other grid setups. For $\Delta\ell = 1$, we have not been able to reproduce this effect which might be due to the fact that we ran into memory limits.

Observation 9. We find the simulation for dynamically adaptive meshes being better suited to Intel Optane technology than a regular grid/fixed mesh setup.

We consider it to be a pattern of many important HPC codes that data access exhibits stream access behaviour close to the compute core—here notably for high orders. On a higher abstraction level, codes however rely on flexible, dynamic tasks and thus do not fit to hardware tailored to stream access. Yet, with many cache levels, the arising non-local data accesses do not hammer the last level memory that often. As long as not too many codes access the memory concurrently, the latency penalty remains under control.

Runtimes should thus intermix computationally heavy and memory-demanding tasks.

While our code exhibits no clear correlation of adaptivity pattern and polynomial order to energy cost in the main memory, we do observe that the usage of Intel Optane technology increases the energy footprint. Future work will have to analyze whether persistent memory modes can bring down these increased energy cost.

Summary and conclusion

Our manuscript studies a non-trivial solver for partial differential equations as we consider it to be characteristic for many upcoming simulation codes: it relies on many tasks of different compute character; the runtime of the tasks and the task composition are hard to predict—adaptive mesh refinement plays a major role here and the situation might become more severe once non-linear equations are solved which require localized Newton or Picard iterations; finally, and the efficiency of the solve hinges on the opportunity to use high polynomial orders and fine meshes. The solver requires massive memory.

Computer memory designers operate in a magic triangle of size, bandwidth and latency. Under given energy and cost constraints, not all three of these characteristics can be improved. While caches optimize for bandwidth and latency, the new Intel memory optimizes for size and bandwidth, while a core increase amplifies NUMA effects—notably for low-order and cheap (Riemann) tasks. As we find our code suffer from memory latency in general, we hypothesized that it may pay off to reduce the core frequency relative to the memory frequency, to use core oversubscription, to hide latency penalties, and to regularize and homogenize all computations, i.e. to work with as regular data structures and task graphs as possible. We have not been able to confirm these hypotheses in general. However, we have found or confirmed attractive alternative solutions or solution proposals per diversity axis.

An increasing flexibility and heterogeneity of clock frequencies allows chips to alter the frequencies for individual system parts. We have not been able to exploit this feature to soothe the impact of latency, although we have confirmed the well-known insight that drastically decreased frequencies improve the energy efficiency of the simulation. Yet, our data suggests that the turbo boost feature of modern chips is of use for very heterogeneous task graphs. It significantly improves the runtime while the energy demands remain under control. It might be reasonable to downclock chips overall, but to allow the runtime to increase the

frequency of particular cores starting from the reduced baseline up to the turbo boost frequency. Notably those cores producing further tasks and running computationally cheap tasks would benefit from such a feature. Such a fine-granular frequency alteration feature—likely coupled with a task runtime—seems to be promising.

An increasing core count and thus NUMA heterogeneity amplify NUMA effects which we label as growing horizontal diversity. Our data suggests that it might be reasonable to subdivide large shared memory chips into logically distributed memory systems. We propose to place multiple MPI ranks on each node. Our benchmarks furthermore clarify that existing cache optimization techniques—notably a high data access localization—continue to pay off. They help to soothe the impact of massively increased latency. In return, however, overbooking is not an option to hide latency/NUMA effects as vendors give up on inclusive caching. It is future work to study whether runtimes explicitly copying data from persistent/large-scale memory into the “right” part of the main memory—which effectively becomes the LLC—can help to eliminate NUMA effects (Kudryavtsev 2018). In this case, future runtimes have to be equipped with the opportunity to predict the task execution pattern and to replace classic prefetching with explicit memory moves.

In the case of ExaHyPE, a homogenized task parallelism which mixes tasks of different compute characteristics allowed us to hide some latency of the Intel Optane technology. Our code has been able to cope with the increased vertical memory diversity. We show that it is absolutely essential to equip tasking systems and algorithms with the opportunity to run memory-intense and compute-bound tasks concurrently, while the majority of compute-intense jobs has to exhibit data access locality. If we get the balance between bandwidth and compute demands right, latency effects remain under control. The access pattern has to be homogenized. Future task systems should internally be sensitive to the compute character of the tasks. They have to mix compute-intense jobs with memory-intense jobs to avoid that a whole node waits for slow deep memory. This naturally can be mapped onto job priorities and mechanisms ensuring that not too many jobs of one priority are launched. To the best of our knowledge, current runtimes as found with OpenMP, TBB or C++11 lack mature support for such priorities or constraints.

Machines equipped with Intel Optane technology provide ample memory. It is an appealing alternative to classic “fat nodes”; also in terms of procurement cost. Once the exascale era makes the total power budget of computers

grow to tens of megawatts, it is an option to trade, to some degree, the DRAM for an energy-modest extra layer of memory. This paper’s experiments navigate at the edge of “fits into the memory” and thus provides too few experimental samples to support claims through frequently observed patterns. We need to run more experiments with more hardware configurations and more applications. Yet, our results suggest that the way forward into the massive-memory age might not be a naïve rendering of the main memory into an additional cache layer; at least not for non-trivial/non-streaming codes. Instead, we ask for three architectural or software extensions: fine-granular frequency control, runtimes with explicit data prefetching, and runtimes with mature task priorities; the latter perhaps even guided by the availability of task data in close caches.

Acknowledgements

The authors appreciate support received from the European Union Horizon 2020 research and innovation programme under grant agreement No 671698 (ExaHyPE). This work made use of the facilities of the Hamilton HPC Service of Durham University. Particular thanks are due to Henk Slim for supporting us with Hamilton. Thanks are due to all members of the ExaHyPE consortium who made this research possible; notably and J.-M. Gallard for integrating aggressively optimised compute kernels into ExaHyPE, and K. Duru, A.-A. Gabriel as well as L. Rannabauer for realising a seismic benchmark on top of ExaHyPE. The authors are particular thankful to Leonhard Rannabauer for the support on running the seismic benchmarks. All underlying software is open source (Bader et al. 2014–2019).

References

- Bader M, Dumbser M, Gabriel A, Igel H, Rezzolla L and Weinzierl T (2014–2019) ExaHyPE—an Exascale Hyperbolic PDE solver Engine. <http://www.exahype.eu>.
- Boyandin K et al. (2018) Guest post: Intel optane and in-memory databases. <https://blog.selectel.com/guest-post-intel-optane-and-in-memory-databases> (obtained 29/08/2018).
- Breuer A, Heinecke A, Rannabauer L and Bader M (2015) High-order ADER-DG minimizes energy- and time-to-solution of seissol. In: *High Performance Computing - 30th International Conference, ISC High Performance 2015, Frankfurt, Germany, July 12-16, 2015, Proceedings*. pp. 340–357.
- Charrier D, Hazelwood B and Weinzierl T (2018) Enclave tasking for discontinuous galerkin methods on dynamically adaptive meshes ArXiv:1806.07984.

- Charrier D and Weinzierl T (2018) Stop talking to me—a communication-avoiding ADER-DG realisation. ArXiv:1801.08682.
- Day S and Bradley C (2001) Memory-efficient simulation of anelastic wave propagation. *Bulletin of the Seismological Society of America* 91(3): 520–531.
- Dumbser M and Käser M (2006) An arbitrary high-order discontinuous Galerkin method for elastic waves on unstructured meshes - II. The three-dimensional isotropic case. *Geophysical Journal International* 167(1): 319–336.
- Glesser D (2016) *Road to exascale: improving scheduling performances and reducing energy consumption with the help of end-users*. PhD Thesis, Grenoble Alpes.
- Hutchinson M, Heinecke A, Pabst H, Henry G, Parsani M and Keyes D (2016) Efficiency of high order spectral element methods on petascale architectures. In: J K, P B and J D (eds.) *High Performance Computing. ISC High Performance 2016, Lecture Notes in Computer Science*, volume 9697. pp. 449–466.
- Kowarschik M and Weiß C (2003) An Overview of Cache Optimization Techniques and Cache-Aware Numerical Algorithms. In: Meyer U, Sanders P and Sibeyn JF (eds.) *Algorithms for Memory Hierarchies 2002*. ISBN 9783540008835, pp. 213–232.
- Kudryavtsev A (2018) Optane and intel memory drive technology, big surprise. <https://itpeernetwork.intel.com/optane-intel-memory-drive-technology> (obtained 10/12/2018).
- McCalpin J (1995) Memory bandwidth and machine balance in current high performance computers. *IEEE Computer Society Technical Committee on Computer Architecture (TCCA) Newsletter* : 19–25.
- Microway (2018) Detailed Specifications of the Intel Xeon E5-2600v4 Broadwell-EP Processors. <https://www.microway.com/knowledge-center-articles/detailed-specifications-of-the-intel-xeon-e5-2600v4-broadwell-ep-processors> (obtained 14/12/2018).
- Reinders J (2007) *Intel Threading Building Blocks*. O'Reilly.
- The SPICE Code Validation (2006) Problem wp2_loh1. <http://www.sismowine.org/model/WP2.LOH1.pdf>.
- Treibig J, Hager G and Wellein G (2010) LIKWID: A Lightweight Performance-Oriented Tool Suite for x86 Multicore Environments. In: *Proceedings of the 2010 39th International Conference on Parallel Processing Workshops, ICPPW '10*. IEEE Computer Society, pp. 207–216.
- Weinzierl T (2018) The Peano software—parallel, automaton-based, dynamically adaptive grid traversals. *ACM Transactions on Mathematical Software* (accepted; arXiv:1506.04496).
- Weinzierl T and Mehl M (2011) Peano—A Traversal and Storage Scheme for Octree-Like Adaptive Cartesian Multiscale Grids. *SIAM J. Sci. Comput.* 33(5): 2732–2760.
- WikiChip (2018) Xeon Gold 6150—Intel. https://en.wikichip.org/wiki/intel/xeon_gold/6150 (obtained 10/12/2018).